Dynamic quantitative phase images of pond life, insect wings, and in vitro cell cultures

Katherine Creath*
Optineering, Tucson, AZ USA 85719; and
College of Optical Sciences, The University of Arizona, Tucson, AZ USA 85721

ABSTRACT

This paper presents images and data of live biological samples taken with a novel Linnik interference microscope. The specially designed optical system enables instantaneous and 3D video measurements of dynamic motions within and among live cells without the need for contrast agents. This "label-free", vibration insensitive, imaging system enables measurement of biological objects in reflection using harmless light levels with current magnifications of 10X (NA 0.3) and 20X (NA 0.5) and wavelengths of 660 nm and 785 nm over fields of view from several hundred microns up to a millimeter. At the core of the instrument is a phase-measurement camera (PMC) enabling simultaneous measurement of multiple interference patterns utilizing a pixelated phase mask taking advantage of the polarization properties of light. Utilizing this technology enables the creation of phase image movies in real time at video rates so that dynamic motions and volumetric changes can be tracked. Objects are placed on a reflective surface in liquid under a coverslip. Phase values are converted to optical thickness data enabling volumetric, motion and morphological studies. Data from a number of different mud puddle organisms such as paramecium, flagellates and rotifers will be presented, as will measurements of flying ant wings and cultures of human breast cancer cells. These data highlight examples of monitoring different biological processes and motions. The live presentation features 4D phase movies of these examples.

Keywords: phase imaging, interference microscopy, polarization interferometry, cellular imaging, cell dynamics, optical thickness measurement

1. INTRODUCTION

The ability to instantaneously measure live cells and follow motions and processes over time provides valuable information to researchers studying cellular dynamics, motility, and cell and tissue morphology. Quantitative phase images can measure structures from interference images analogous to those viewed with phase-contrast imaging and differential interference contrast imaging. These images can reveal features and quantitative data that are not available through conventional imaging. Phase imaging measures optical thickness variations due to small variations in refractive index relating to variations in density of different structures and materials within cells and tissues. Very small refractive index variations can manifest as large variations in phase images. Phase image data enable quantitative measurements that aren't possible with standard microscopy techniques. Samples do not need to be stained, labeled or marked, and harmless light levels are used. By taking short snapshots, adding the dimension of time opens up the ability to track motions of cells, see how cells interact with one another, and follow small motions within cells, tissues and structures.

This paper presents a number of measurements taken using a breadboard polarization Linnik interference microscope specially designed for measurement of biological samples in liquids under coverslips. Objects are viewed in reflection; however, the method is easily adaptable to measurement in transmission or for use with immersion.

* email: kcreath@ieee.org

The motivation behind designing this system was to develop a research tool to study dynamic cell behavior in a way that is not harmful to live cells so processes could be monitored in real time. This paper presents many examples of dynamic phase measurements of biological samples.

2. BACKGROUND

Full-field phase-imaging interference microscopes have been around since the early 1980's.[1-3] High precision measurements on small surfaces have been obtained for engineering surfaces such as hard disk substrates, magnetic heads for hard drives, and critical dimension measurement for lithography.[3] Techniques developed for these instruments have relied upon phase-measurement methods, which predominantly obtain interferograms sequentially, and therefore require good vibrational damping, and static specimens so that high-quality data can be obtained. Most interferometric microscopes have utilized narrowband illumination with short coherence lengths of tens of microns. The reason for narrowband "low coherence" illumination is to reduce effects of reflections off of nearby surfaces and to help reduce effects of speckle in the imaging systems. With biological samples, low coherence illumination enables the samples to be isolated in space without getting spurious interference patterns from other surfaces (mainly the coverslip). These techniques have been used for biological measurements but have not been utilized as much as they could because most of them are sensitive to motion and vibration. [4-14]

As an alternative, pixelated phase mask sensor technology uniquely provides a single frame phase measurement in a compact, robust format that is compatible with conventional microscope imagining systems, and permits the use of a wide variety of wavelengths and source bandwidths.[15-17] It enables the creation of a versatile and compact microscope interferometer for biological applications. These sensors have been implemented in many different types of interferometers and are insensitive to vibration and do not require scanning. All necessary information to determine phase is recorded in a single snapshot.[15-17]

2.1 Linnik interference microscope

The interference microscope used for this work is based upon a Linnik configuration (see Sec 2.1.1).[3] It is comprised of a Köhler-type illumination utilizing a low coherence extended source,[18] and a simple imaging system as shown in Figure 1. An aperture stop enables controlling the size of the source in the entrance pupil of the microscope objectives, while a field stop enables easier alignment of the system.

This particular design utilizes polarized light so that the object and reference beams have orthogonal polarizations. The incoming illumination is split into orthogonal polarizations before the microscope objective using a polarization beamsplitter. The relative irradiances of the test and object beam are balanced for maximum contrast using the polarizer. A quarter-wave plate (QWP) before the camera combines the two polarized beams so that the two beams can interfere at the pixelated phase mask (see Sec 2.2).

The extended source reduces coherent noise, noise from spurious reflections, and enables isolation of a small depth region within the sample. A sample in water or cell media is viewed in reflection through a cover slip.

For the work presented in this study, sources with wavelengths of 785 nm and 660 nm were used with 10X NA 0.3 and 20X NA 0.5 objectives. The imaging "tube" lens magnification was either 1X or 1.67X.

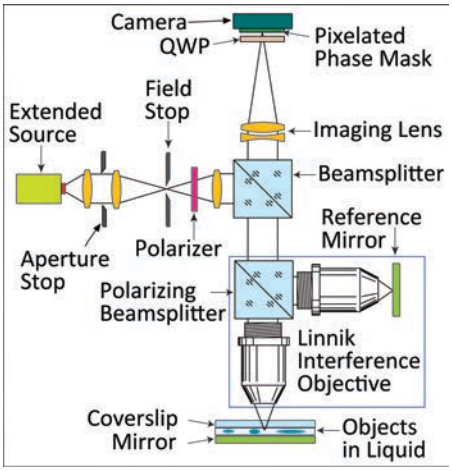

Figure 1. Optical schematic of Linnik interference microscope.

2.1.1 Linnik interference objective

For a Linnik interference microscope objective, the reference objective and the reference mirror are moved together to match the path lengths in the reference and test arms to maximize fringe contrast (see Figure 2). When imaging an object, first focus is adjusted on the sample. Then the reference arm is moved to maximize fringe contrast. The reference mirror once aligned relative to the reference objective should not need to be readjusted. And when measuring a series of samples with the same coverslip and liquid thickness, this should not need be to readjusted.

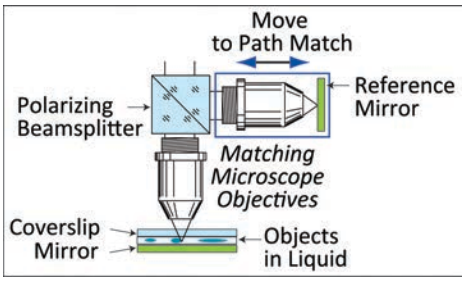

Figure 2. Linnik interference microscope objective.

The coverslip and liquid thickness will cause there to be some spherical aberration in the measurements. However, because it is possible to subtract out small amounts of spherical aberration or to subtract a reference measurement, there is no noticeable image degredation with magnifications of 20x or lower. There will be some optical dispersion due to the coverslip and liquid, but these are not a problem with the source chosen for this system. At 20X and ~1/2 mm total thickness, fringe contrasts of 0.5-0.6 are easily obtainable.

2.1.2 Extended low coherence source

For this study, laser with wavelengths of 785 nm and 660 nm were utilized as sources. To reduce the spatial coherence to 25-35 µm, the laser beam was focused onto a rotating ground glass diffuser and then coupled into a multi-mode optical fiber. The laser can either be temporally coherent or have coherence lengths in the hundreds of microns. What's important is that there needs to be sufficiently high temporal coherence over a path length differences that take into account the cover glass.[19, 20] A temporally low coherence source like an LED would require equal optical paths (cover slips and liquid) in both arms of the Linnik so that the temporal coherence function overlaps with the spatial coherence function.

2.1.3 Breadboard microscope

Figure 3 shows the breadboard layout of the microscope with the source off to the left and the camera at the top. The configuration is a down-looking reflective microscope. The Linnik interference objective points down at the object with the reference arm parallel to the table. The sample can be manipulated relative to the microscope with an x-y-z-tip-tilt 5-axis stage.

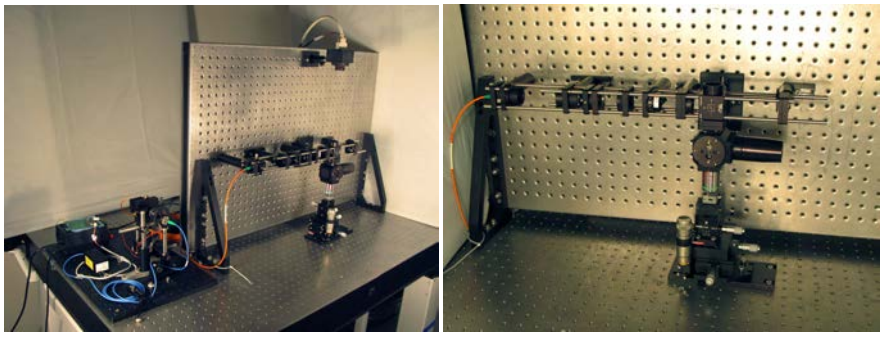

Figure 3. (left) Breadboard microscope with source on left and camera at top. (right) Close-up of body of microscope showing Linnik interference objective pointing down towards a 5-axis stage.

2.2 Measuring phase using a pixelated phase mask

2.2.1 Wire-grid polarizers

The polarization-mask is constructed from an array of micropolarizers that are constructed from wire grid polarizers as shown in Figure 4. Wire-grid polarizers are made of tiny metal wires that are deposited on a

transparent substrate (typically aluminum wires on a glass substrate). The linewidth, thickness and period of the wires are approximately 100nm, 120nm and 240nm respectively **(**see Figure 4**).** These sub-wavelength structures have the property of reflecting light polarized parallel to the wires and transmitting light polarized perpendicular to them. Thus, they function as a very efficient polarizer over a wide range of wavelengths and angles. Most significantly, the wires are deposited on the substrate using a photolithographic process (similar to semiconductor manufacturing) permitting orientation of the wires at arbitrary angles within multiple regions on the substrate.

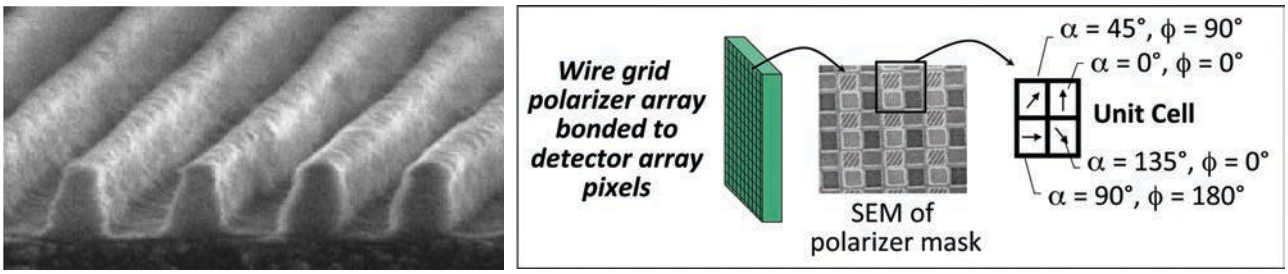

Figure 4. (left) SEM micrograph of wire grid polarizer section (Courtesy of Moxtek). (right) Pixelated phase mask sensor is an array of wire grid micropolarizers on a glass substrate bonded to the detector array. The phase mask is comprised of 4 different polarizations comprising a unit cell of 2x2 different phase shifts as noted above.

2.2.2 Phase imaging with a pixelated phase-mask

Figure 4 illustrates how the micropolarizers are spatially distributed and oriented in the pixelated polarization mask manufactured by 4D Technology. The operation of the mask as an instantaneous interferometer can be understood as follows. When the reference and test beams are combined, each having orthogonal circular polarization (i.e., right-hand circular and left-hand circular), the measured intensity at each pixel of the mask is given by [21]

$$I(x,y) = \frac{1}{2}\left\{ I_r + I_s + 2\sqrt{I_r I_s}\cos\left[\Delta\varphi(x,y) + 2\alpha_p\right]\right\},$$

where α_p is the angle of the polarizer with respect to the *x, y* plane, I_r and I_s are the intensity of reference and signal beams respectively, and $\Delta\phi(x,y)$ is the optical path difference between the beams. From this relation it can be seen that a polarizer oriented at zero degrees causes interference between the in-phase (i.e., 0°) components of the incident reference and signal beam. A polarizer oriented at 45° interferes the in-phase quadrature (i.e., 90° or $\pi/2$) component. A polarizer oriented at 90° interferes the out-of-phase (i.e., 180° or π) component. Finally, a polarizer oriented at 135° interferes the out-of-phase quadrature (i.e., 270° or $3\pi/2$) component.

Thus, the signal measured at each sensor pixel is given by its transfer function, the phase-difference between the reference and test beams, and the amplitude of each beam. For each of the four pixel types we can write,

$$A(x,y) = \frac{1}{2}\left\{ I_r + I_s + 2\sqrt{I_r I_s}\cos\left[\Delta\varphi(x,y)\right]\right\} \qquad C(x,y) = \frac{1}{2}\left\{ I_r + I_s + 2\sqrt{I_r I_s}\cos\left[\Delta\varphi(x,y) + \pi\right]\right\}$$

$$B(x,y) = \frac{1}{2}\left\{ I_r + I_s + 2\sqrt{I_r I_s}\cos\left[\Delta\varphi(x,y) + \frac{\pi}{2}\right]\right\} \quad D(x,y) = \frac{1}{2}\left\{ I_r + I_s + 2\sqrt{I_r I_s}\cos\left[\Delta\varphi(x,y) + \frac{3\pi}{2}\right]\right\}.$$

Multiple interferograms can thus be synthesized by combining pixels of each phase type. The resulting four interferograms can be processed by a variety of algorithms that are well-known in the art for calculating phase difference.[22, 23] For example, a possible implementation for measuring phase difference is a simple four-bucket algorithm, e.g.,

$$\varphi(x,y) = ATAN\left\{\frac{\left[C(x,y) - A(x,y)\right]}{D(x,y) - B(x,y)}\right\},$$

where the values A, B, C, and D are taken from adjacent neighboring pixels. This produces a modulo 2π (wrapped) phase which then needs to be unwrapped using standard techniques.[24] Thus, a real-time phase image can be produced.

2.3 Measuring optical thickness

2.3.1 What are we measuring?

This type of microscope directly measures phase, specifically the phase difference between the reference beam and the test beam, also known as optical path difference (OPD). Each interference fringe in reflection corresponds to one-half wave of OPD. Typically, the raw units of this measure are in terms of wavelengths of the source light (waves).

To make these data more useful we convert the phase data to optical thickness OT(x,y) which is given by

$$OT(x,y) = OPD \cdot \frac{\lambda}{2} = \phi(x,y)\left[\frac{\lambda}{4\pi}\right]$$

$$OT(x,y) = n(x,y,z) \cdot t(x,y,z)$$

Optical thickness (OT) is an integrated measure of the overall path through the sample. For viewing in reflection it involves a double pass through the coverslip and liquid containing the objects. Denser areas of the object with higher indices of refraction will yield a larger OT as shown in Figure 5. Typically, the index of refraction of the coverslip is ~1.5, the index of water is ~1.33, while cellular media is ~1.37, cytoplasm ~1.39 and cellular organelles like nuclei ~1.41-1.43. Subtle differences as small as the third decimal place in refractive index are detectable by this system.[25]

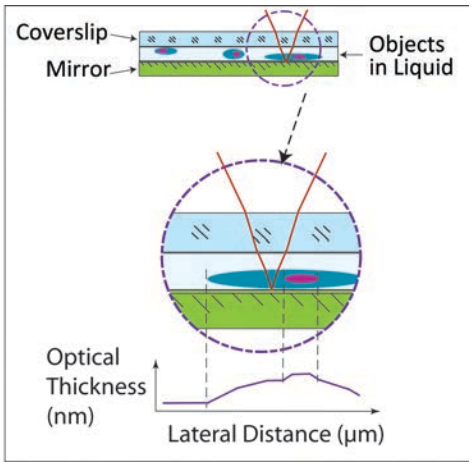

Figure 5. Path length through test sample including coverslip, liquid and objects. Graph (bottom) shows optical thickness profile for the section within the highlighted area.

2.3.2 Following motion with dynamic measurements

To illustrate dynamic quantitative phase-image movies, subtle changes in water temperature were measured across a 50mm field of view using a low coherence Twyman-Green interferometer with a 4D Technology phase-measuring camera in a horizontal configuration. The object was a plexiglass cuvette with 5 mm thick walls and a chamber 20 x 35 x 5 mm. The cuvette was filled with warm water and a drop of cold water was added using a dropper. Figure 6 presents a series of 4 images taken 0.1 sec apart as the drop enters the cuvette. The top row (A) shows the irradiance (intensity) on the sensor – what you would normally see as a brightfield image. The drop can be seen at the top of the first image and a faint outline of the drop is seen in the second; however, it is not possible to see the drop in the last 2 images. The second row (B) shows the interference fringes.

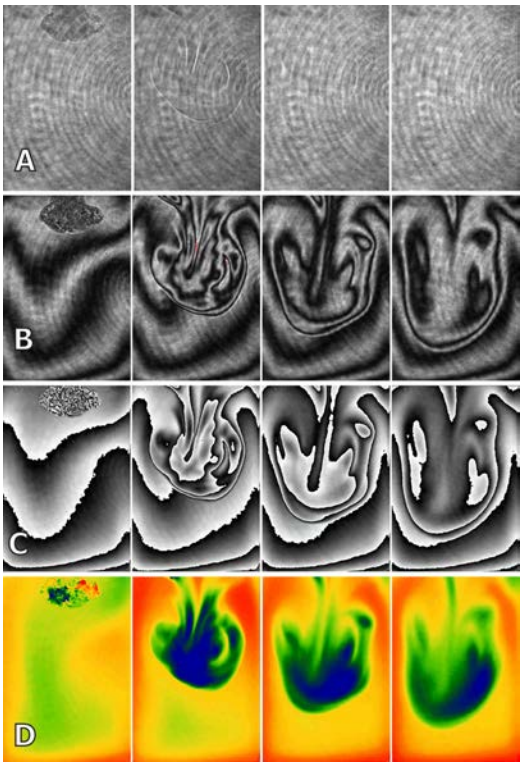

Figure 6. Phase-image frames of cold water drop dropped into cuvette of warm water. Object size is 20 x 35 mm taken at 0.1 sec intervals. (A) Bright-field image. (B) Interference fringes. (C) Wrapped phase modulo 2π. (D) Phase images with a range (high-low) of 1.75 waves.

Notice that there are some variations in the background phase, but the drop is easily visible in each of the frames. What the fringes represent is the phase deviation owing to a slightly smaller refractive index for the cold water than that of the warm water. The third row (C) presents the wrapped (modulo 2π) phase obtained from the last Equation of Section 2.2.2. Discontinuities in these images are due to the modulo 2π nature of the arctangent (ATAN) function. The final step of the phase measurement process is to unwrap the phase and remove these 2π ambiguities. This is done using an algorithm that traces a path and adds or subtracts multiples of 2π until differences between adjacent pixels are less than π (see for example [24]). The bottom row (D) contains the phase images. The color scale from high to low goes from red to orange to yellow to green to blue. Blue is a shorter optical path difference (OPD) and colder relative to red. With the quantitative phase map it is easy to discern the water drop in each image. The range of phase deviation for the cold-water drop is about 1.75 waves at 660 nm or about 1.15 µm. As an example showing the quantitative deviation in terms of optical thickness, Figure 7 shows a profile through the center of the second phase image in Figure 6(D).

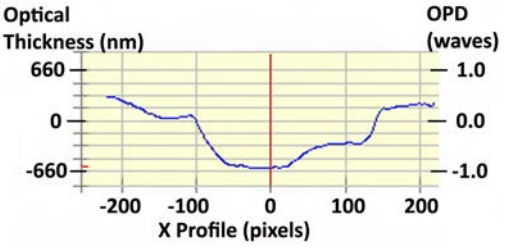

Figure 7. X cross-section profile of line through center of 2nd phase image in Figure 6(D).

2.3.3 Potential applications

There are many potential applications of this type of imaging. Some have been described in the literature (see, for example [4-14]). This vibration insensitive design is especially effective when dynamic motions and changes over time need to be tracked. Quantitative data enables volumetric studies as a function of time while exposing cells to different environments or while studying apoptosis. Variations in morphology and shape can be followed with time during cellular processes. Dynamics of tissues and cells like nerve cells and muscle fibers can be measured quantitatively in real time while applying perturbations. Mechanism and processes of cell death (apoptosis) or cell division can be imaged and quantified dynamically. Therapeutic modalities such as photodynamic therapy can be studied to characterize effects. As an example, tracking of individual cells or cellular organelles can be accomplished by following features in dynamic phase images to determine where to deliver the photodynamic beam. There are many other possible applications.

3. DYNAMIC PHASE IMAGES

The rest of this paper focuses on showing examples of images of different types of biological and cellular samples. In the live presentation, movies were shown illustrating the dynamic quality of these measurements. Unfortunately, in a printed medium, these movies cannot be shown. Instead, to show the dynamics of these measurements, time series are shown with a few snapshots during the motion. To get a current html link to see movie files on line, please email the author.

3.1 Pond life

The first series of images is from a culture made from dirt in a mud puddle. This culture was fed with organic material like dead grass and sugar. Over the course of a few weeks, a number of different species came to life in this pond scum. These included many types of paramecium, voticella, amoeba, stentors, euglena, peranema, chlamydomonas, and rotifers. A few of these images are shown below.

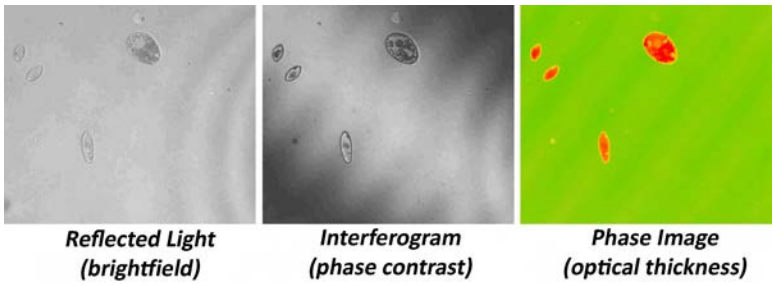

Figure 8. Images of paramecium. (left) Brightfield image in reflection. (center) Interference image. One of 4 channels used to determine the phase image (right). Areas that are red are thicker than those that are green. See Figure 9 for color scale.

3.1.1 Paramecium

Paramecium are simple one-celled organisms. At 10X with a 660 nm source they can easily be resolved. We have seen them as small as specs up to 10-20 µm in size. Figure 8 and Figure 9 show one large and 3 medium sized paramecium as they are swimming around in a 400 µm field of view. Notice that organelles inside the paramecium are easily resolved. These images are a few frames taken from a 20-frame movie sampled every 0.1s.

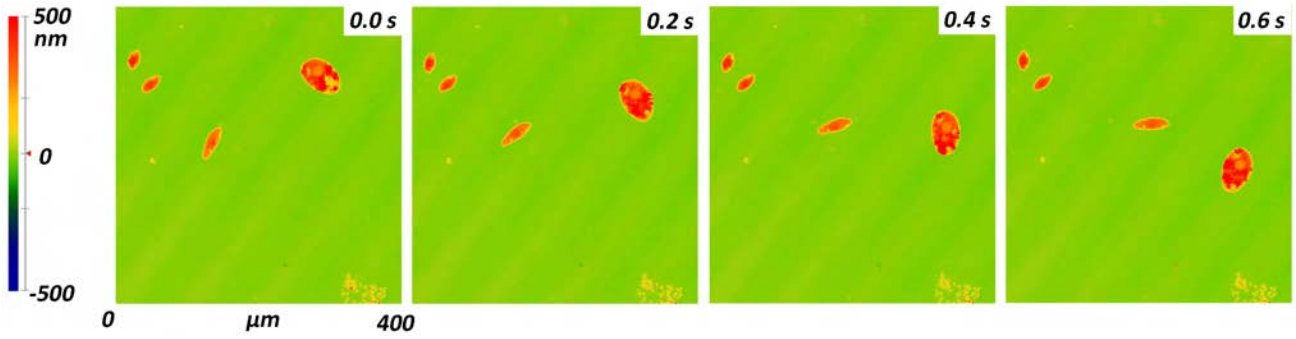

Figure 9. Sequence of images showing paramecium swimming with ~2 ms exposure times at 10X. These are samples from a movie containing 20 frames taken over 2 seconds. Images can be taken as quickly as 30 frames/sec.

Paramecium encyst themselves (roll up into balls) when they begin to dry out so that they can hibernate until there is more water when they come back to life. Figure 11 shows an average of 20 measurements of paramecium encysting taken at 10X with a 785 nm source. Notice that the optical thickness quantifies the cell densities at various portions of the cells and that the organelles are easily visible. Averaging helps increase the signal-to-noise but requires the objects to be stationary.

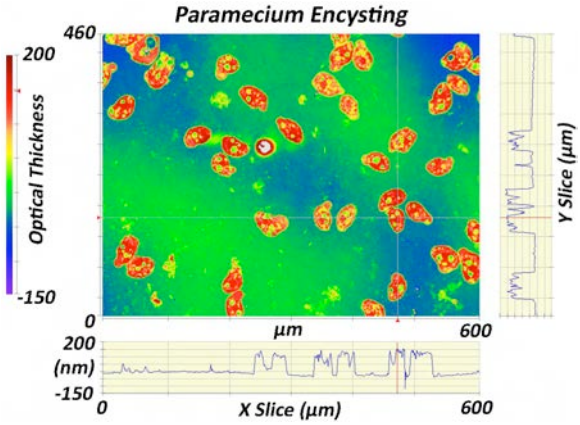

Figure 11. Phase image of paramecium as they encyst while drying out. X and Y profiles through the hairline cursors are shown along the sides.

3.1.2 Rotifers

Rotifers are the most complex organism growing in this mud puddle culture. They are comprised of about a thousand cells. If you've ever watched them under a microscope you'll notice that they have a tail with 2 protrusions that they used to push off from (see lower right of Figure 10) and a mouth with cilia around edges to sense and grab food such as paramecium (see upper left of Figure 10). Rotifers have very flexible bodies and change their shape as they are moving in sometimes radical ways.

A phase image comprised of a 20-frame average is shown in Figure 10 taken at 10X with a 785 nm source. The pseudocolor scale ranging over 1000 nm is set to bring out detail inside the rotifer. The optical thickness of this sample is about 1200 nm maximum to minimum (peak-to-valley).

Two images out of a sequence of 20 images taken over ~2 seconds are shown in Figure 12. This rotifer is digesting something in its stomach. The rotifer motion is noticeable between the images and details of internal organs are easy to see. These were also taken at 10X with a 785 nm source.

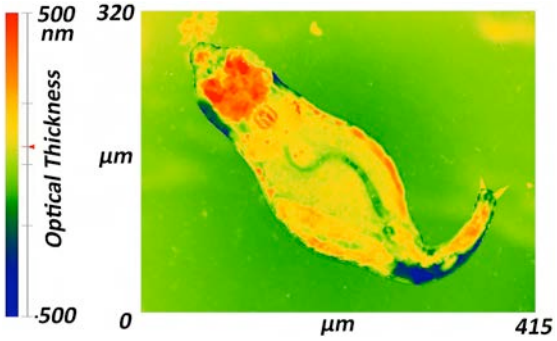

Figure 10. Phase image of 20 frame average of a still rotifer taken at 10X with a 785 nm source. Pseudocolor scale on left shows a 1 µm range of optical thickness.

3.1.3 Flagellates

Flagellates utilize flagella for motility to help them sense and move. One common type of flagellates are uni-cellular chlamydomonas. They are a type of green algae. Figure 13 shows a sequence of images of a flagellate. The organism is spinning and the flagellum is moving significantly between frames. These are samples from a 3.5 s movie with 3 ms exposures. Motion between images is similar to what it looks like with a time scale of 0.1 s intervals. The flagellum is about 5 µm in diameter and about 80-100 µm long. The pseudocolor scale has been set with limits that bring out the flagellum while clipping the maximum (red) and minimum (blue) optical thickness values of the body and organelles.

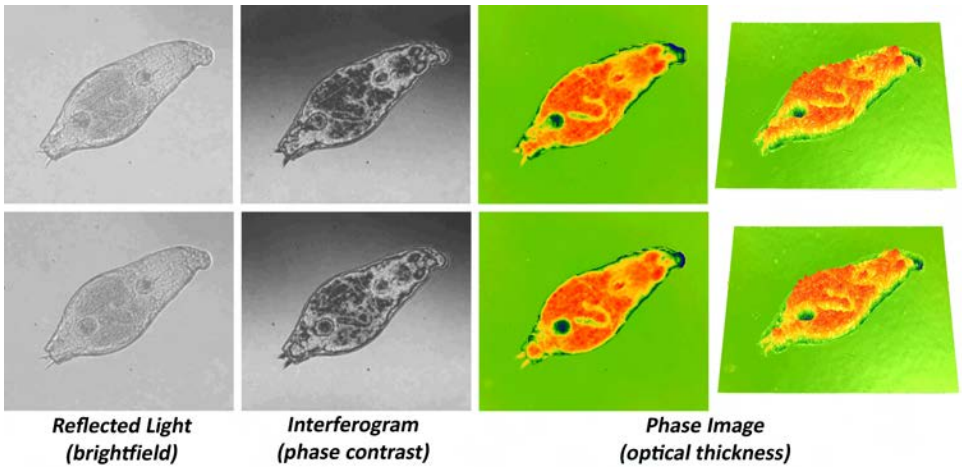

Figure 12. Two snapshots from a movie of a slowly moving rotifer taken fractions of a second apart. (far left) Brightfield images. (left) Interference images. (right) Phase image showing optical thickness. (far right) 3D view of phase image.

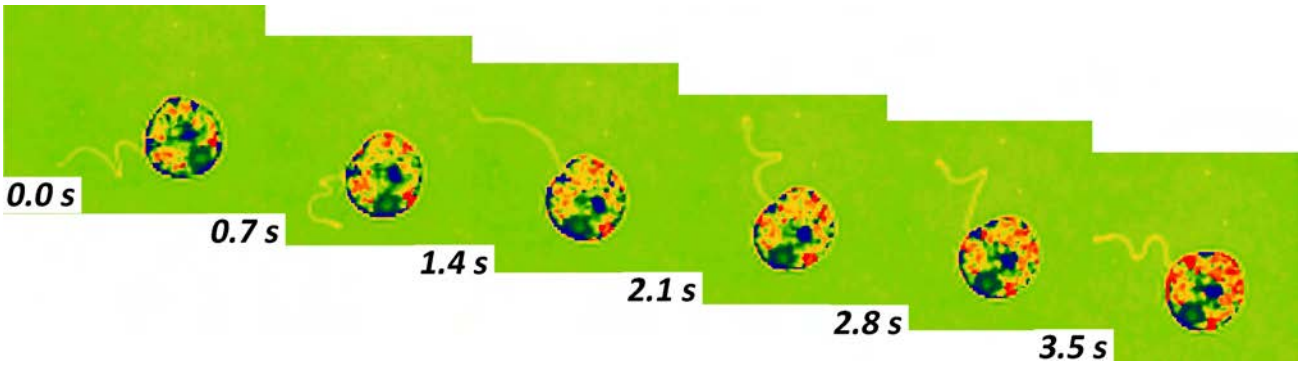

Figure 13. Flagellate with a body ~40µm in diameter taken at 10X with a 660 nm source. Note detail of flagella motion.

3.2 Insect wings

Insect wings were measured as an example of the ability to quantify optical thickness of a translucent tissue sample from a more complex organism. These images are of a leaf-cutter ant wing (*Acromyrex versicolor).* Figure

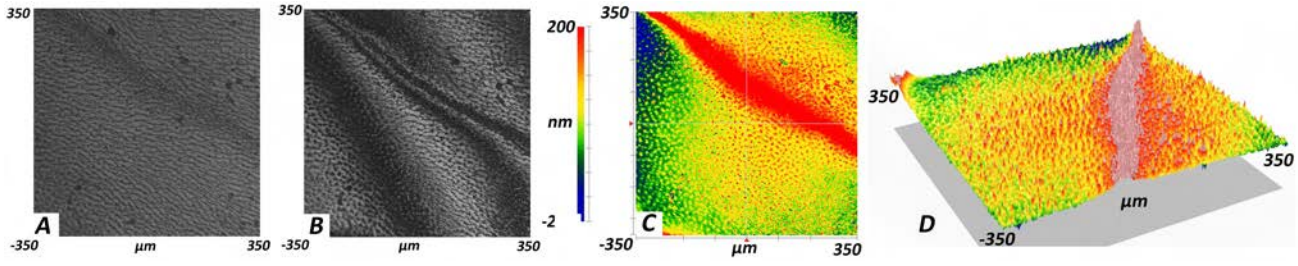

Figure 14. Images of a flying ant (*Acromyrex versicolor)* wing section taken at 10X with a 660 nm source and ~2ms exposures. (A) Brightfield image. (B) Interference image (phase contrast). (C) Phase image (optical thickness) in psuedocolor. (D) 3D view of (C).

14 shows brightfield, interference and phase images of a 350 µm square wing section taken at 10X with a 660 nm source. Notice hairs sticking up from the wing as well as the thicker structure of the wing scaffold.

3.3 Cell cultures

3.3.1 In vitro human breast cancer cell culture

Cell cultures of the MCF715 human breast cancer line were grown in cell media on coverslips. To image these cells, the coverslips were flipped over and placed onto of a highly reflective mirror with cell media filling in between the mirror and coverslip. These images were taken at 20X with a 1.67X tube lens, a 660 nm source and 2 ms exposures. Cell cultures can also be measured directly on glass slides with media and a coverslip, but for the same short exposure time would require a more powerful source.

Figure 15 shows an image of some of these cells. Note that the intercellular matrix and cilia around the edges of the matrix are clearly visible and easily resolved as are organelles and nuclei within the cells. The lateral sampling in the image for this exposure is 0.53 µm for each 4 pixel 2x2 cell in the pixelated phase mask. The optical resolution at NA=0.5 is 0.8 µm (0.61 λ/NA) yielding a slightly oversampled image. To process this image so that different optical thickness layers have different colors, the background shape due to the mirror and coverslip has been subtracted out by fitting piston, tilt, curvature and cylinder from the areas where there are not cells present.[23]

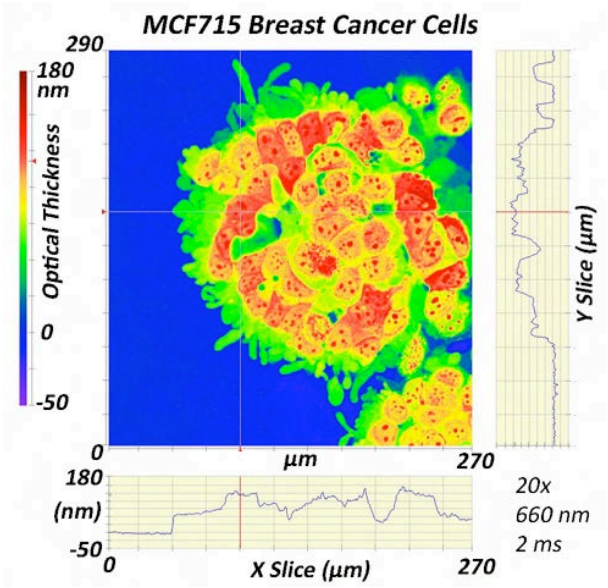

Figure 15. Culture of human breast cancer cell line grown on a coverslip taken at 20X with a 660 nm source.

Another area of the cell culture is shown in Figure 16. Here there are fuzzy portions between cells that are forming new cells and the matrix along with cilia forming around the edges of the clumps.

Figure 17 shows the cells of Figure 15 after contact with purified water and then a KCL solution. There is noticeable osmotic swelling of the cells while the cilia have shriveled. Notice that hardly anything is visible in brightfield, while the interference image shows definite detail that is brought out in the quantitative phase images.

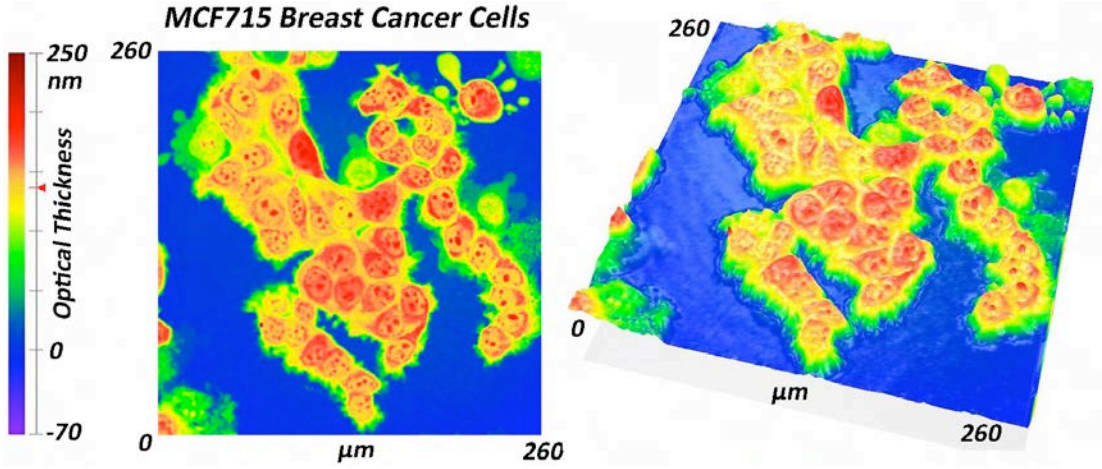

Figure 16. Phase images showing contour and 3D view of human breast cancer cells. Notice cells and matrix forming that look fuzzy without organelles.

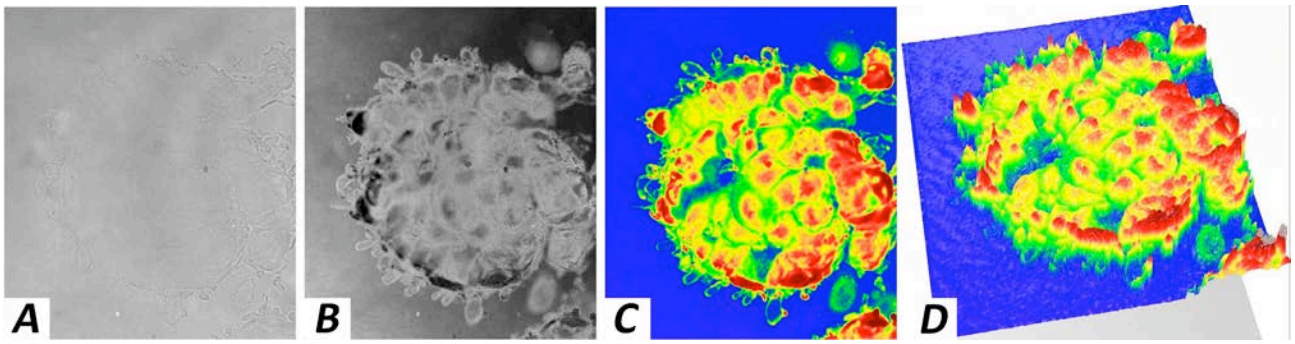

Figure 17. Human breast cancer cells of Figure 15 after contact with purified water and then a KCL solution. (A) Brightfield image. (B) Interference image similar to phase contrast. (C) Phase image with pseudo-color representation of optical thickness scaled from -50 to 220 nm (a slightly larger scale than Figure 15). Notice osmotic swelling of cells and shriveling of cilia compared to Figure 15. (D) 3D plot of (C).

3.3.2 Dynamic studies of in vitro cell cultures

Figure 18 shows some images of another cell culture of human breast cancer cells after contact with various media. All of these images are scaled in optical thickness to the same limits of -100 to 450 nm so that changes are more obvious. In Figure 18(A) the cells are in their growth media. In Figure 18(B) the cells have been exposed to purified water causing them to osmotically swell. Figure 18(C) shows how they further swell and flatten after further exposure to purified water while Figure 18(D) shows the cells after then being exposed to NaOH. For each of these cases, 4D phase movies were recorded showing changes every few seconds. Changes are obvious as seen in these few images. The movie is more dramatic.

After this series of images, the cells were then exposed to Alconox® (a detergent containing enzymes). Once the cells have osmotically swelled from purified water and begun breaking down by NaOH, the Alconox® further breaks down the cell walls and the cells dissolve. Figure 19 shows a series of images from a longer 4D phase movie taken as the cells were dissolving. The movie images were taken every 4 seconds over a 78 second time span while Figure 19 shows snapshots every 10 seconds. With more time resolution it is possible to watch how the cells break down and dissolve.

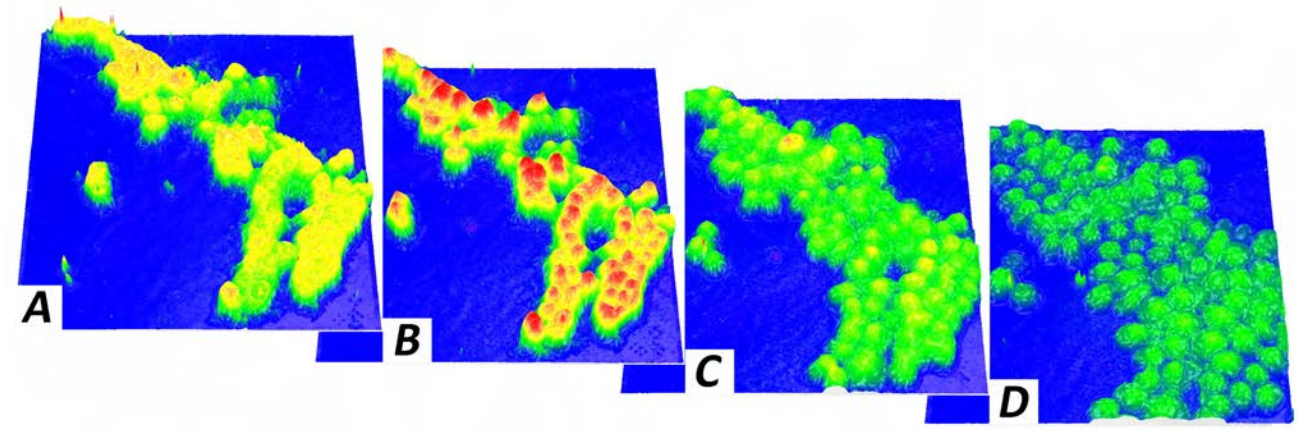

Figure 18. 4D time series of 3D phase images of another breast cancer cell culture. All images have the same optical thickness pseudocolor scale from -100 to 450 nm. (A) Cells in original media. (B) After contact with purified water the cells osmotically swell. (C) After more purified water the cells continue to swell and flatten. (D) After contact with NaOH the cells are beginning to break down. Processes can be monitored with specified time delays as short as 30 frames per second. These are a sampling of movies taken with sampling times of a few seconds over several minutes.

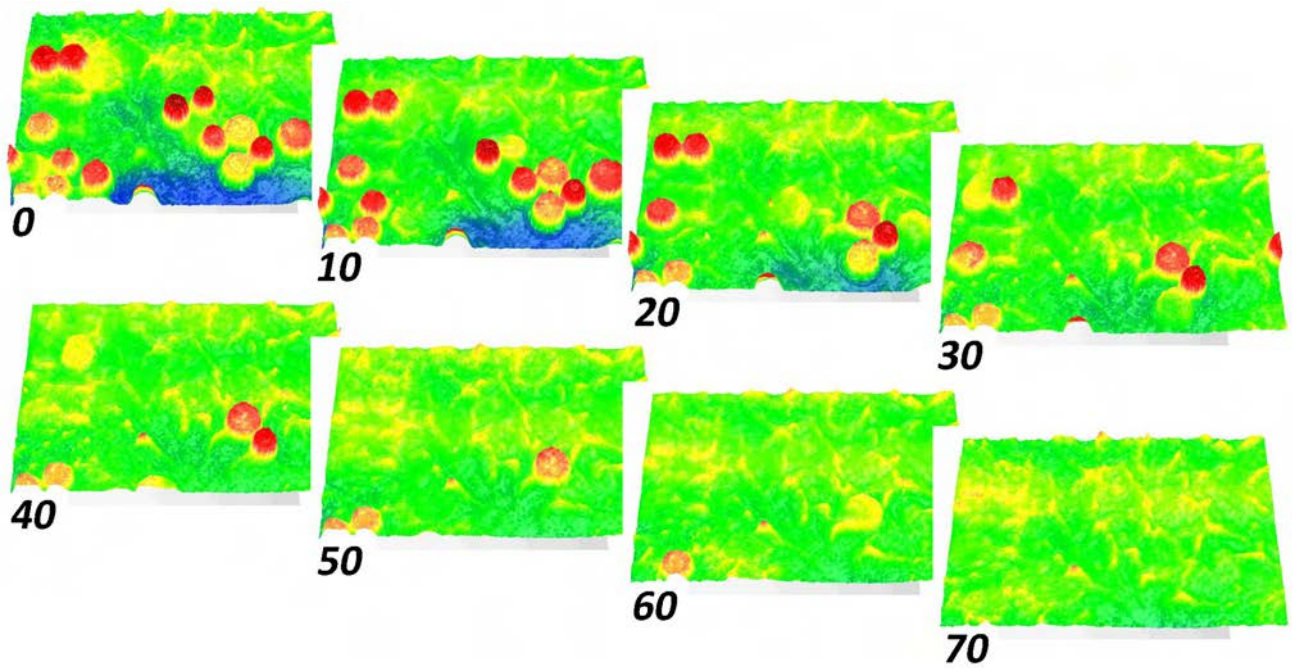

Figure 19. 4D time series of phase images of breast cancer cells as they dissolve after contact with pure water, NaOH and Alconox®. Imaging area is 200 x 300 µm. Data are taken as 20X with a 660 nm source and 2 ms exposures. Samples above are every 10 seconds from a 78 second long movie. The P-V (peak-to-valley or maximum-to-minimum) is -120 to 120 nm.

4. DISCUSSION AND CONCLUSIONS

This paper has shown a number of examples of 4D phase measurements of living biological organisms and how they may be tracked dynamically as they move or as perturbations are made to their environment. The short exposure times freeze motion instantaneously and since all data to determine phase and optical thickness can be gathered in a single snapshot, no scanning is necessary. Harmless light levels along with no need for staining, labeling or marking cells offers a non-destructive means of observing and quantifying biological behavior and dynamic variations over time. The ability to dynamically measure biological organisms in real time opens up many different types of applications ranging from flow cytometry to tissue dynamics, morphological and volumetric studies along with mechanistic studies, process monitoring, quantification of cellular motion, monitoring and tracking cellular damage under known perturbations, tracking cell migration, nerve and muscle transmission, histology and photodynamic therapy. This model can also be extended to higher magnifications, immersion objectives, higher numerical apertures, a large range of wavelengths, and viewing cells in transmission as well as reflection. Data from brightfield imaging and phase contrast (interference image) are also obtained simultaneously along with phase and optical thickness. Conceptually, this model could be further modified to include simultaneous fluorescence measurements to more specifically track specific mechanisms.

5. ACKNOWLEDGEMENTS

The author wishes to thank Dr. James Millerd and Mr. Neal Brock of 4D Technology Corporation for use of the phase imaging camera and 4Sight software as well as Dr. Andrew Rouse and Dr. Arthur Gmitro of The University of Arizona Department of Radiology for cell samples and networking with other researchers. This work was partially supported by NIH/NCRR (1R43RR028170-01).

6. REFERENCES

1. G. E. Sommargren, "Optical Heterodyne Profilometry," Applied Optics **20**, 610-618 (1981).
2. J. C. Wyant, C. L. Koliopoulos, B. Bhushan, and O. E. George, "An optical profilometer for surface characterization of magnetic media," ASLE Trans. **27**, 101-113 (1984).
3. J. Schmit, K. Creath, and W. James C, "Ch. 15. Surface Profilers, Multiple Wavelength, and White Light Intereferometry," in *Optical shop testing*, D. Malacara, ed. Wiley-Interscience, Hoboken, N.J., 667-755, (2007).
4. G. A. Dunn, and D. Zicha, "Phase-Shifting Interference Microscopy Applied to the Analysis of Cell Behaviour," Symposia of the Society for Experimental Biology **47**, 91-106 (1993).
5. D. Zicha, and G. A. Dunn, "AN IMAGE-PROCESSING SYSTEM FOR CELL BEHAVIOR STUDIES IN SUBCONFLUENT CULTURES," Journal of Microscopy-Oxford **179**, 11-21 (1995).
6. B. Eppich, J. Beuthan, C. Dressler, and G. Muller, "Optical phase measurements on biological cells," Laser Physics **10**(2), 467-477 (2000).
7. V. P. Tychinsky, A. V. Kretushev, I. V. Klemyashov, T. V. Vyshenskaya, N. A. Filippova, N. T. Raikhlin, and A. A. Shtil, "Quantitative real-time analysis of nucleolar stress by coherent phase microscopy," Journal of Biomedical Optics **13**(6), 064032 (2008).
8. C. Yang, A. Wax, M. S. Hahn, K. Badizadegan, R. R. Dasari, and M. S. Feld, "Phase-referenced interferometer with subwavelength and subhertz sensitivity applied to the study of cell membrane dynamics," Optics Letters **26**(16), 1271-1273 (2001).
9. G. Popescu, "Quantitative Phase Imaging of Nanoscale Cell Structure and Dynamics," in *Methods in Nano Cell Biology, Volume 90*, B. P. Jena, ed. Elsevier, San Diego, 87-115, (2008).
10. D. O. Hogenboom, C. A. DiMarzio, T. J. Gaudette, A. J. Devaney, and S. C. Lindberg, "Three-dimensional images generated by quadrature interferometry," Optics Letters **23**(10), 783-785 (1998).
11. W. S. Rockward, A. L. Thomas, B. Zhao, and C. A. DiMarzio, "Quantitative phase measurements using optical quadrature microscopy," Applied Optics **47**(10), 1684-1696 (2008).
12. J. Reed, M. Frank, J. J. Troke, J. Schmit, S. Han, M. A. Teitell, and J. K. Gimzewski, "High throughput cell nanomechanics with mechanical imaging interferometry," Nanotechnology **19**(23), (2008).
13. G. J. Ross, A. W. Bigelow, G. Randers-Pehrson, C. C. Peng, and D. J. Brenner, "Phase-based cell imaging techniques for microbeam irradiations," Nuclear Instruments & Methods in Physics Research Sec B **241**(1-4), 387-391 (2005).
14. L. F. Yu, S. Mohanty, G. J. Liu, S. Genc, Z. P. Chen, and M. W. Berns, "Quantitative phase evaluation of dynamic changes on cell membrane during laser microsurgery," Journal of Biomedical Optics **13**(5), (2008).
15. N. J. Brock, J. E. Millerd, J. C. Wyant, and J. B. Hayes, "Pixelated phase-mask interferometer ", USPTO, ed. 4D Technology Corporation, United States, (2007).
16. B. T. Kimbrough, "Pixelated mask spatial carrier phase shifting interferometry algorithms and associated errors," Applied Optics **45**(19), 4554-4562 (2006).
17. M. Novak, J. Millerd, N. Brock, M. North-Morris, J. Hayes, and J. Wyant, "Analysis of a micropolarizer array-based simultaneous phase-shifting interferometer," Applied Optics **44**(32), 6861-6868 (2005).
18. M. Born, and E. Wolf, *Principles of Optics* Pergamon Press, Oxford, (1975).
19. I. Abdulhalim, "Competence between spatial and temporal coherence in full field optical coherence tomography and interference microscopy," J Opt A: Pure Appl. Opt. 8, 952-958 (2006).
20. V. Ryabukho, and D. Lyakin, "Longitudinal pure spatial coherence of a light field with wide frequency and angular spectra," Optics Letters 30(3), 224-226 (2005).
21. M. P. Kothiyal, and C. Delisle, "Shearing interferomter for phase-shifiting interferometry with polarization phase-shifter," Applied Optics **24**(24), 4439-4442 (1985).
22. K. Creath, "Phase-measurement interferometry techniques," in *Progress in Optics*, E. Wolf, ed. Elsevier Science Publishers, Amsterdam, 349-393, (1988).
23. D. Malacara, M. ServÌn, and Z. Malacara, *Interferogram analysis for optical testing* Taylor & Francis, Boca Raton, FL, (2005).
24. D. W. Robinson, "Phase unwrapping methods," in *Interferogram Analysis*, D. W. Robinson, and G. T. Reid, eds. IOP Publishing, Bristol, 194-229, (1993).
25. K. Creath, and G. E. Schwartz, "Dynamic visible interferometric measurement of thermal fields around living biological objects," in *Interferometry XII: Techniques and Analysis*, K. Creath, and J. Schmit, eds. SPIE - The International Society for Optical Engineering, Bellingham, WA, 24-31, (2004).